

# Learning to Infer Parameterized Representations of Plants from 3D Scans

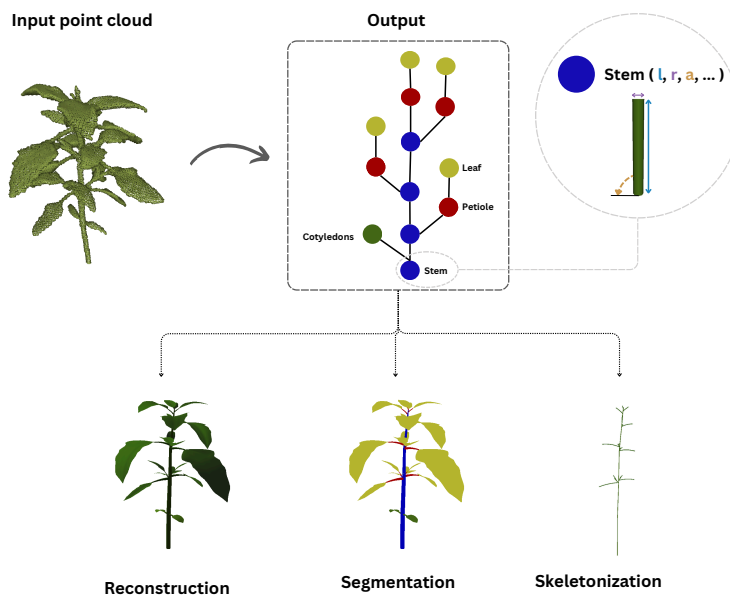
Samara Ghrer<sup>1</sup>Christophe Godin<sup>2</sup>Stefanie Wuhrer<sup>1</sup>

Figure 1: Our method takes a 3D point cloud of a plant as input, and outputs a parameterized representation of the plant. This representation encodes the plant’s branching structure and geometry along with semantic information such as organ type, and allows for multiple tasks including reconstruction, organ segmentation and skeleton extraction.

## Abstract

Reconstructing faithfully the 3D architecture of plants from unstructured observations is a challenging task. Plants frequently contain numerous organs, organized in branching systems in more or less complex spatial networks, leading to specific computational issues due to self-occlusion or spatial proximity between organs. Existing works either consider inverse modeling where the aim is to recover the pro-

cedural rules that allow to simulate virtual plants, or focus on specific tasks such as segmentation or skeletonization. We propose a unified approach that, given a 3D scan of a plant, allows to infer a parameterized representation of the plant. This representation describes the plant’s branching structure, contains parametric information for each plant organ, and can therefore be used directly in a variety of tasks. In this data-driven approach, we train a recursive neural network with virtual plants generated using an L-systems-based procedural model. After training, the network allows to infer a parametric

<sup>1</sup>Inria centre at the University Grenoble Alpes

<sup>2</sup>Inria centre of Lyon

tree-like representation based on an input 3D point cloud. Our method is applicable to any plant that can be represented as binary axial tree. We evaluate our approach on *Chenopodium Album* plants, using experiments on synthetic plants to show that our unified framework allows for different tasks including reconstruction, segmentation and skeletonization, while achieving results on-par with state-of-the-art for each task.

# 1 Introduction

Inferring high-level information of plants from observations in a way that respects the biological traits (e.g. the radius of a lateral branch is never larger than that of its parent stem) is an important problem that has been studied for decades [52]. High-level information includes the reconstruction of the 3D geometry of a plant, the segmentation of a plant into parts, and the extraction of a skeleton or measurements. Observations are typically 2D images or 3D scans. Automatically extracting this information allows to use reconstructed 3D plants in content generation and virtual reality [29], and to use part segmentation, skeleton information, and measurements in plant phenotyping, e.g. [33, 13, 18].

The problem of inferring high-level information is challenging because plants have complex structures due to their branching systems, which leads to strong self-occlusions and ambiguities. Existing works that analyze 2D or 3D plant observations therefore either focus on inverse modeling, where the goal is to find growth rules that allow to generate a given plant, or are task-specific. Inverse modeling is challenging and existing methods are limited to simple branching structures [24, 48]. Task-specific methods focus on 3D reconstruction e.g. [29], organ segmentation e.g. [33], skeletonization e.g. [13], or measurement extraction e.g. [18].

We propose a unified approach that, given a 3D scan of a plant, allows to infer a parameterized representation of the plant. This representation contains parametric information on each plant organ, and can therefore be directly used to reconstruct the 3D geometry of the plant with corresponding segmentation

labels and measurements, thereby allowing to solve a variety of tasks. We achieve this by learning a shape space of 3D plants based on representations generated by a biologically inspired procedural model, in a way that for any point in shape space, we can retrieve its corresponding parameterized representation. By learning a function that maps an observed 3D point cloud to the learned shape space, our work allows to find the representation of a plant without reconstructing the full procedural model rules. Hence, our work can be considered a step towards inverse modeling-based reconstruction.

The key idea that allows our method to address the challenging problem of inferring high-level information from 3D scan data plagued by occlusions is to learn a shape space with the help of instances generated using a procedural model made of recursive rules that describe the development of the plant architecture. We leverage a Lindenmayer-systems (L-systems) model [40] allowing to generate plants, and the recursive nature of plant growth in a recursive neural network to learn a latent distribution of the plants’ geometry and branching structure. We generate a synthetic dataset using procedural modeling rules, which allows for supervised learning from large amounts of occlusion-free training data. The synthetic plants are represented in a binary axial tree form that can be geometrically interpreted to obtain the 3D virtual plant. The binary tree format is exploited using a recursive auto-encoder. To address the problem of generalizing to 3D scans plagued by acquisition noise and occlusions, we virtually simulate the acquisition noise on the 3D virtual plants, in addition to simulated monocular depth maps during training and learn a mapping from simulated 3D scan data to the shape space.

We evaluate our method on synthetic *Chenopodium Album* plants, an annual plant, in early growth stages. We choose this plant because of the availability of real scans in dataset [34], and its simple structure in early stage that can be encoded into a binary tree representation. We use our method to perform the different tasks of 3D reconstruction, skeleton extraction and plant part segmentation. Our experiments show results that are on-par with the state-of-the-art, with more robustness to noisy

and partial inputs. We also show qualitative results for instance segmentation, and discuss the potentials to apply our method on real scans.

The main contributions of this work are:

- A unified approach to infer a parameterized representation of a plant from a 3D scan based on a recursive neural network.
- 3D plant reconstruction, skeletonization, organ segmentation, with performance that is on-par with the state-of-the-art on each task.
- A dataset of virtual plants, in a form of L-Strings, that represents instances of *Chenopodium Album* plants in early growth stages.

## 2 Related Work

Vision based systems and platforms have been developed for plant phenotyping and crops analysis [7, 8, 11, 10, 37]. Furthermore, plant scan datasets and data generation methods were provided for training data-driven models, e.g. the rosebush annotated dataset ROSE-X [15], an annotated dataset of 3 plant species PLANEST-3D [31], and a labeled point cloud generation method of virtual plants [4]. Furthermore, small datasets of 3D scans were captured e.g. [34].

Existing works on plant phenotyping that deal with plant scan data belong to two main categories: works that aim for inverse plant modeling, and task-specific methods that aim to extract information. Our work is in between these categories, since it is centered around the inference of parameterized plant representations, which allows to extract various high-level information including the full branching structure and 3D geometry of the plant. This can be seen as a step towards inverse plant modeling as we infer an instance of a procedural model.

### 2.1 Inverse Plant Modeling

Procedural plant models generate a plant following growth rules. On the contrary, inverse plant modeling aims to find the rules that allow to generate the given

plant. In other words, the goal is to infer the model given the plant geometry as input. Guo et al. [23] and Štáva et al. [47] infer procedural modeling rules generated using an L-system from 2D images of simple branching structures. Štáva et al. [48] introduce a parametric procedural model and estimate the parameters that allow this model to generate trees of a single species similar to an input 3D mesh. More recently, Lee et al. [24] used transformers to learn a latent space that allows to predict L-system rules that correspond to 3D point clouds of a tree, and to generate similar trees.

As Lee et al. [24], we use data-driven neural networks to learn a latent representation of the plant. However, we aim to directly predict the L-String that represents the input plant with its branching structure, geometrical and other biological traits, instead of predicting the L-system rules.

### 2.2 Task Specific Methods

Existing methods used in plant phenotyping from 3D input point clouds mainly focus on four tasks: 3D reconstruction of the plant, extracting a skeleton of the branching structure of the plant, segmenting the plant into organs, and extracting measurements from the point cloud.

**3D Reconstruction** Reconstructing plant geometry from an input scan represented by a 3D point cloud is an important problem due to its applications in computer graphics and plant phenotyping. This is a particularly challenging 3D reconstruction problem as plants contain thin structures and as different organs lead to significant self-occlusions.

In computer graphics, Gonzalez et al. [22] use UnrealEngine [41] to reconstruct digital urban trees by reconstructing a mesh that represents the tree trunk, estimating the volume and density of the canopy, and filling the canopy with generated leaves. This method focuses on global geometry and ignores the branching structure of the plant architecture.

Another line of work focuses on the tree branching structure [14, 39, 54, 29, 53], by estimating a skeletal structure of the tree. Given the skeleton, a mesh surface can be reconstructed over each branch. However,

the foliage part of the trees is either excluded from the input, or reconstructed by randomly generating leaves to fill the canopy.

Closest to our work, Prasad et al. [38] explore different implicit surface reconstruction algorithms, including classical and neural based ones, on 3D point clouds of a single plant. They demonstrate that this task is challenging due to fine geometric structures. Note that our method’s output contains more information than a 3D reconstruction, as our parametric output allows to infer information on the plant’s skeleton and organs. For 3D reconstruction, we compare our method experimentally to this work.

**Skeletonization** Extracting the skeletal structure of plants is a well-studied problem. One line of works, discussed above, extracts skeletons as one part of a pipeline to reconstruct the plant [14, 39, 54, 29, 53].

Another line of works corresponds to optimization-based methods. Meyer et al. [32] use a point contraction algorithm to extract skeletons of leafless cherry trees. Works using graph-based approaches have shown to extract skeletal structures even in the presence of noise for trees [53, 30]. A recent deep learning-based approach uses a sparse convolutional neural network to estimate the medial axis of a tree [13]. Given a point cloud of a plant with an initial extracted skeleton, Chaudhury et al. [6] propose a stochastic optimization to refine the initial skeleton by estimating point transformations.

All discussed methods require a leafless input point cloud to estimate the skeleton. When leaves are present in the input point cloud, these methods estimate skeletal structures inside of the leaves, thereby adding noise to the output. Since our method outputs a segmented parameterized representation of the plant, extracting the skeleton of a leafy input plant does not pose additional challenges. We experimentally compare our method to one successful approach from each category for which code is available, namely [53, 30, 6].

**Segmentation** Segmenting different organs from point clouds of plants is critical for phenotyping on both semantic and instance levels. Both learn-

ing and optimization-based techniques were proposed in the literature to segment a plant into organs. Mirande et al. [33] propose a graph-based optimization approach with botanical knowledge refinement for semantic and instance segmentation. Wabzada et al. [51] present an unsupervised data-driven method using histogram clustering in a Euclidean space. For supervised learning methods, a benchmark for plant organ segmentation [49] has been released based on the ROSE-X dataset [15]. More complex deep learning architectures designed for organ segmentation lead to accurate results [26, 50, 25]. We compare our method experimentally to two of these successful approaches [26, 25].

**Measurement Extraction** Extracting phenotypic measures like leaf area index or main stem height provides insight about plant and crop behavior in different conditions. Paproki et al. [36] propose a mesh processing technique for 3D plants phenotypic traits analysis from multi-view images. Chattopadhyay et al. [3] model and reconstruct apple trees with diameter estimation for the application of automatic dormant pruning. Ghahremani et al. [18] apply the RANSAC algorithm to model plant organs that fit an input point cloud to estimate phenotypic features like angles and diameters of leaves and branches.

**Positioning** Our experiments focus on the three tasks of 3D reconstruction, skeletonization and segmentation. As shown in Table 1, only few works perform the three tasks of 3D reconstruction, skeletonization and segmentation, like [29, 54]. However, these methods are designed to be applied on big trees with trunks and foliage, and are not applicable on small annual plants where the leaf size to stem diameter proportion is different. On annual plants, our method remains generic due to the learned parametric model that contains the information needed for different tasks.

### 3 Background

We propose a method that learns a shape space of a plant species with the help of recursive neural net-

Work	Recon- struction	Skeletoni- zation	Segment- ation	Annual plants
Gonzalez et al. [22]	✓	✗	✓	✗
Liu et al. [29]	✓	✓	✓	✗
Du et al. [14]	✓	✓	✗	✗
Linvy et al. [30]	✓	✓	✗	✗
Preuksakarn et al. [39]	✓	✓	✗	✗
Parsad et al. [38]	✓	✗	✗	✓
Dobbs et al. [13]	✗	✓	✗	✗
Chaudhury et al. [6]	✗	✓	✗	✓
Yan et al. [54]	✓	✓	✓	✗
Meyers et al. [32]	✗	✓	✓	✗
Mirande et al. [33]	✗	✗	✓	✓
Turgut et al. [49]	✗	✗	✓	✓
Turgut et al. [50]	✗	✗	✓	✓
Wahabzada et al. [51]	✗	✗	✓	✓
Li et al. [26]	✗	✗	✓	✓
Li et al. [25]	✗	✗	✓	✓
Paproki et al. [36]	✗	✗	✓	✓
Ghahremani et al. [18]	✗	✗	✗	✓
Ours	✓	✓	✓	✓

Table 1: Positioning of our method w.r.t. the ability to perform 3D reconstruction, skeletonization and part segmentation, and the applicability on small annual plants.

works. To learn this shape space, we rely on a large dataset of 3D plants with corresponding parametric representations that has been simulated with the help of plant models. This section provides background on plant modeling and on recursive neural networks.

### 3.1 Plant Modeling

Plant modeling aims to find a mathematical model that describes the complex geometry and growth rules for a species of plants. Moreover, plant models respect biological rules to allow realistic simula-

tion of the plant’s appearance and behavior in different environmental conditions [5, 19]. The importance of plant modeling comes from its applications in biological and agronomical studies. The synthetic models can be used to perform growth simulation experiments, or estimate biological traits and growth patterns of plants. This allows to study plants with fast and non-invasive methods.

Procedural methods are among the most commonly used plant modeling approaches, including L-systems [40], the space colonization algorithm [43], and commercial tools such as SpeedTree. In our work, we use procedural plant models to generate data for training and evaluating our neural network.

Our implementation uses an L-system-based procedural approach [40] to generate plant data, a classical rule based plant modeling technique, that is particularly convenient due to the availability of tools such as L-Py [2]. In L-systems, a plant is represented as a string of symbols, called L-String, possibly bearing geometrical or biological parameters. Similarly to natural or computer language grammars, an L-system consists of a set of rewriting rules that define how plant components represented by L-String symbols change as time proceeds, by specifying how symbols get replaced by combinations of other symbols [40, 21]. At each step, the rules replace the symbols in parallel, resulting in a new L-String representing the next plant state.

L-Strings of plants mainly consist of two types of symbols: modules and brackets. Modules can refer to various plant parts e.g. stems, leaves, flowers, etc. Opening and closing brackets indicate the start and the end of every branch in the plant. Two successive modules in an L-string have a parent-child relationship. Open brackets allow for a module to have more than one child, and for different children to have siblings relationships. However, each parent has at most one special child that corresponds to its successor on the same plant axis. Such L-Strings encode axial trees [40] that represent the plant’s architecture. Modules in L-Strings can have parameters that give information about a plant organ. This includes the organ’s age, order in the branch or geometric attributes (e.g. length, radius, angle, etc.). By applying geometric interpretation rules on an L-String us-

ing turtle geometry [1], a 3D scene of the plant can be generated. The virtual plant comprises of connected 3D shapes corresponding to the modules. In other words, an L-String can encode a plant’s geometry in addition to its architecture.

Our L-system models are implemented using the L-Py [2] language, that provides an extension of the Python programming language to design procedural models using the L-systems formalism. L-Py allows to create and manipulate L-system rules, handle the information present in an L-String, and generate 3D virtual plants from L-Strings.

### 3.2 Recursive Neural Networks

Recursive Neural Networks (RvNN) [12] are a class of deep neural networks that apply the same network architecture recursively on input that is structured as a tree graph to give a single representation in a latent space. The term *recursive* refers to the network architecture being applied to the output of step  $i - 1$  during step  $i$ . The recursivity of RvNNs allows to handle input of varying size, as the network is applied in a bottom-up fashion from the leaves to the root. These networks learn hierarchical dependencies and correlations between input components.

Socher et al. [46, 45] introduced an RvNN that learns information on different domains, including natural language processing and natural scene image processing, by recursively parsing a tree graph with binary structure. Models based on RvNN have been applied to natural language processing [9], 3D indoor scene generation [28, 17], blood vessel synthesis [16], and 3D shape structure recovery [35], segmentation [55] and generation [27].

Of particular interest for our work are recursive auto-encoders for binary trees, such as the ones used to generate 3D shapes of man-made objects [27]. A recursive auto-encoder learns on a binary tree structure, where all nodes can be represented in a latent space of dimension  $dim_S$ . The encoder follows the tree structure and recursively merges pairs of inputs to form a new point in the same latent space until the full tree is represented as a single point in latent space. Inversely, the decoder recursively decodes a single point into two points in the same latent space

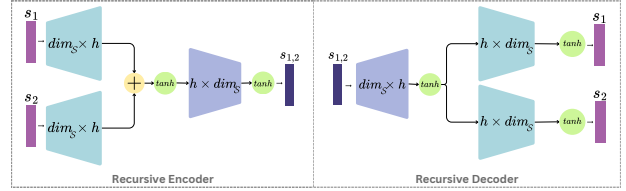


Figure 2: The network architectures used for the recursive encoder and decoder. A binary tree structure is recursively encoded into latent space  $\mathcal{S}$ . Latent points  $s_1 \in dim_S$  and  $s_2 \in dim_S$  are merged into  $s_{1,2} \in dim_S$  by the encoder. Symmetrically, the decoder splits  $s_{1,2}$  into two latent points  $s_1$  and  $s_2$ .  $dim_h$  denotes the dimension of the hidden layer.

until the full tree structure is decoded.

Figure 2 shows an example of the network architecture of a recursive encoder-decoder pair. The encoder-decoder pair allows to learn correlations between continuous properties encoded in features along the tree. An RvNN typically contains different types of encoder-decoder pairs. This allows to implement different operations, such as merging or splitting different parts.

During decoding, given a point in latent space, an algorithm is needed to decide which decoder to apply and when to stop the recursion. To achieve this, the encoders and decoders are trained with ground truth structural information. During encoding, the information of which encoder to apply is available. For decoding, the RvNN jointly learns a set of classifiers that is applied before each decoding step.

L-Strings have tree-like hierarchical structure, and we use RvNNs to encode them into latent points while capturing the relationships between the different modules, and their features’ correlations along the tree. We also use RvNNs in the opposite direction, to retrieve the tree structure and its parameters.

## 4 Method

### 4.1 Overview

We aim to obtain a tree-like parametric representation  $l$  in the form of an L-String from an input point cloud  $P$  that stems from an unstructured 3D scan of a plant. Learning a direct regression from the space of 3D point clouds to the space  $\mathcal{L}$  of L-Strings is a difficult problem, as the point clouds have varying number of points and are unstructured, and as the L-Strings varies both in discrete (i.e. number and type of modules) and continuous (i.e. values of the parameters describing angles and lengths) ways.

To address this problem, we combine an RvNN learned on  $\mathcal{L}$  with an encoder that maps a point cloud to  $\mathcal{S}$ , as shown in Fig. 3. During training, we first learn the latent space  $\mathcal{S}$  that allows to represent L-Strings of a fixed plant species. This allows to represent 3D plants of varying shapes, with different number of organs, and different skeletal structures using latent representations  $s \in \mathcal{S}$ , and is explained in Sec. 4.2. Second, we train a neural network called point cloud encoder that maps an input point cloud  $P$  to a point  $s \in \mathcal{S}$ , as outlined in Sec. 4.3). During inference, the input point cloud  $P$  is encoded in the latent space as a point  $s$  using the point cloud encoder, and subsequently decoded to an L-String using the recursive decoder, as detailed in Sec. 4.4.

### 4.2 Representing L-Strings in Latent Space

We aim to learn a latent space  $\mathcal{S}$  that allows to represent various static instances of the same species of plant. Plants are represented in the space of L-Strings  $\mathcal{L}$  and can be generated with a set of L-System rules. However, the branching structure of the L-Strings may not always correspond to a binary tree structure. We therefore first simplify the L-Strings by summarizing the information of modules that always occur together in the plant species. The resulting combined modules are called nodes in the following, and we design the combination rules to guarantee a binary tree structure after combination. To simplify notations, we call the simplified L-String  $l \in \mathcal{L}$  in the

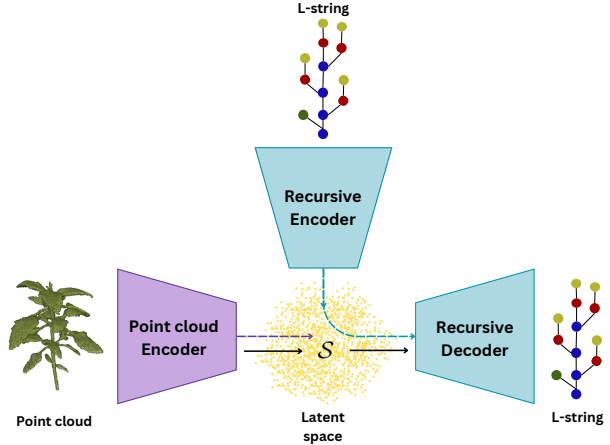


Figure 3: Overview: our method learns a latent space  $\mathcal{S}$ , that allows the mapping of 3D point clouds to L-Strings. At inference, the point cloud is mapped to  $\mathcal{S}$  using the point cloud encoder on the left, and the resulting latent point allows to reconstruct the corresponding L-String using the L-String decoder on the right.

following.

Our goal is to learn an encoder function  $E : \mathcal{L} \rightarrow \mathcal{S}$ , and a decoder function  $D : \mathcal{S} \rightarrow \mathcal{L}$ , such that  $l \approx D(E(l))$ ,  $\forall l \in \mathcal{L}$ .

Learning to encode different shape and structural information in latent points of fixed dimension is challenging. Inspired by [27], we use an RvNN to learn the hierarchical relations between the modules of the L-String, leveraging the recursive nature of plant structures [20].

To achieve this, each node of the tree is represented individually in a point in the latent space,  $s_i \in \mathcal{S}$ , using a node auto-encoder. In a second step, each subtree of the L-String is represented in  $\mathcal{S}$  using a recursive auto-encoder. This procedure is carried out recursively from the tree-graph leaves up to its root.

#### 4.2.1 Node Auto-encoders

Each type of node has a different set of parameters, e.g. angles, widths, radii. This results in nodes that have different dimensionality in general, and that are not directly comparable. To allow nodes with different number of parameters to be used as

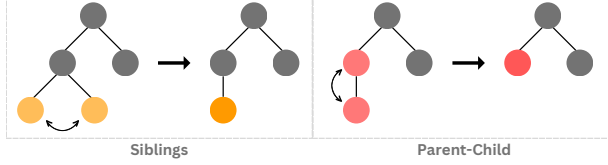


Figure 4: The two criteria to merge/split points in latent space shown on an example tree. Merging is applied recursively in a bottom-up manner until the whole tree is merged into one point, while the splitting performs the inverse operation.

input in an RvNN, we first map the information of each node to  $\mathcal{S}$ . To achieve this, a node encoder-decoder pair is learned for each node type. In the following, let  $E_{node,i}$  and  $D_{node,i}$  denote the encoder and decoder for each type of node, with  $i = 1, \dots, N$  and  $N$  the number of types of nodes. Both  $E_{node,i}$  and  $D_{node,i}$  consist of a fully connected linear layer, followed by a  $\tanh$  activation.

#### 4.2.2 Recursive Auto-encoders

After applying node encoding, an input L-String is represented as a binary tree where all nodes are individually represented as points in  $\mathcal{S}$ . It can then serve as input to an RvNN auto-encoder. To recursively merge or split the nodes, we design encoder-decoder pairs based on the relationship of the input nodes in the tree. Two nodes to be merged can be either siblings or have a parent-child relationship in the tree.

Based on this observation, we consider the two merging/splitting criteria shown in Figure 4. For each criterion, we learn one recursive encoder-decoder pair. Both the sibling encoder-decoder ( $E_{sib}, D_{sib}$ ) and the parent-child encoder-decoder ( $E_{pc}, D_{pc}$ ) are implemented as shown in Fig 2.

#### 4.2.3 Auxiliary Classifiers

In addition to the encoder-decoder pairs, it must be decided how to properly split the points to reconstruct the L-String structure. Each point in  $\mathcal{S}$  is either a result of a merging process by one of the recursive encoders ( $E_{sib}, E_{pc}$ ), or it represents an individual node. For the RvNN to decode structural in-

formation, it needs to learn to choose the appropriate decoder ( $D_{sib}, D_{pc}$ ), or to end the recursive splitting. To predict the right decoder, we associate classes for the different splitting options (siblings, parent-child, stop) and jointly train a classifier on them.

Due to different node types, the network should needs to learn which node decoder  $E_{node,i}$  to apply to reconstruct each node of the L-string. For that, a second classifier is trained, that allows to predict the node type for a latent point  $s$  that is fully split. This classifier, called  $C_{node}$  has  $N$  output classes.

Both classifiers share the architecture of a two-layer fully connected neural network. The first layer maps the input latent point to a hidden representation using a linear transformation followed by a  $\tanh$  activation. The second layer maps the hidden features to an output vector that corresponds to the different classes.

#### 4.2.4 Training

All auto-encoders are trained by minimizing a reconstruction loss at the node level. For node  $n$  in L-String  $l$ , with a set of parameters, the reconstruction loss  $L_{rec}(n)$  is the mean squared error between the input node parameter vector that contains the plant part information and its reconstruction. The reconstruction loss for the full L-String is

$$L_{rec} = \sum_n L_{rec}(n). \quad (1)$$

At each recursive encoding step  $i$ , the output point  $s$  is a result of merging two points  $(s_1^{(i)}, s_2^{(i)})$ . Then in the inverse decoding step,  $s$  will be split into  $(\hat{s}_1^{(i)}, \hat{s}_2^{(i)})$  that are supposed to represent the same information as  $(s_1^{(i)}, s_2^{(i)})$  and should fall in the same region in  $\mathcal{S}$ . To learn a structured representation space into which we can map information from another modality (point clouds), we encourage corresponding latent points during encoding and decoding to be located close-by in  $\mathcal{S}$  using a step-based recursion loss  $L_{step}$  that is defined as

$$L_{step} = \sum_i \left( \left( s_1^{(i)} - \hat{s}_1^{(i)} \right)^2 + \left( s_2^{(i)} - \hat{s}_2^{(i)} \right)^2 \right). \quad (2)$$



The classifiers are trained with softmax classification and cross entropy loss.  $C_{split}$  takes a latent point  $s$  as input, and predicts one of the three classes: parent-child split, siblings split or leaf node (no split).  $C_{node}$  predicts one of  $N$  possible node types. We denote the cross entropy losses used to train these classifiers by  $L_{split}$  and  $L_{node}$ , respectively.

Finally, the total loss that is used for training the recursive L-String auto-encoder is

$$L_{total} = L_{rec} + L_{step} + L_{split} + L_{node}. \quad (3)$$

### 4.3 Point Cloud Encoder

After representing L-Strings in latent space  $\mathcal{S}$  has been learned, 3D plants can be represented as latent points  $s \in \mathcal{S}$ , and  $s$  can be decoded into an L-String parametric representation  $l$ . To allow retrieving an L-String  $l$  from an input point cloud  $P$ , we learn a new mapping function  $E_{points}$  from the space of point clouds to  $\mathcal{S}$  using a PointNet architecture [42].

To train  $E_{points}$ , we take advantage of paired input data, for which we are given both the point cloud  $P$  and its corresponding L-String  $l$ . Passing  $l$  through the recursive L-String encoder produces a latent point  $s$ . By applying  $E_{points}$  on  $P$ , we obtain  $\hat{s}$ . The training optimizes the loss function

$$L_{points} = \sum_j (\hat{s}_j - s_j)^2, \quad (4)$$

where  $j$  loops over all samples in the training set. This loss encourages the point cloud encoder function  $E_{points}$  to represent  $P$  at the location  $\hat{s} \in \mathcal{S}$  that represents its corresponding L-String  $s$ .

### 4.4 Inferring L-Strings from Input Point Clouds

At inference, the input is an unstructured point cloud  $P$ . This input is encoded in  $\mathcal{S}$  using the point cloud encoder, and the resulting point is decoded using the recursive decoder as  $l = D(E_{points}(P))$ .

Errors in the predicted module parameters of the reconstructed L-String can have a propagating effect on the global geometry of the plant reconstruction. For example, errors in predicting the angle of a

stem that is located in the bottom of the plant can lead to deviation in the plant growth axis along the main stem. To avoid such deviations, we align the reconstructed plant with the input in an optimization framework. We optimize on certain parameters of the stem modules starting from the ones at the bottom of the plant and going up. This optimization is done on the angle and length parameters for the *Chenopodium album* plants, minimizing the one-sided Chamfer Distance from the reconstructed stem to the input point cloud. We then optimize on the parameters of the individual leaf modules that define the leaf size and curvature. The latter optimization is applied on the leaves in no particular order, minimizing the single directional Chamfer Distance between the reconstructed plant and the input point cloud. This results in a parametric L-String representation  $l$  that allows for various downstream phenotyping tasks. In this paper, we focus on the following tasks.

**3D Reconstruction** can be solved directly by applying the geometric interpretation rules on  $l$  to retrieve the virtual plant 3D scene.

**Skeletonization** is solved by applying geometric interpretation rules drawing organ skeletons on  $l$ .

**Segmentation** is solved by applying geometric interpretation rules on  $l$  and by keeping the labels of the organ types. The labels are propagated to  $P$  by assigning each point in  $P$  the most frequently assigned label among its  $k$  nearest neighbors in the annotated point cloud corresponding to  $l$ .

## 5 Dataset

To train and evaluate our method, we design and generate a synthetic dataset of L-String and point cloud pairs of the *Chenopodium Album* plant. First, we generate the L-Strings using LPy platform [2], with L-system production and geometric interpretation rules, that we optimize to generate realistic *Chenopodium* virtual plants. We define different time functions for the different plant parameters that

guide the plant growth for a range of [12, 19] days to get *Chenopodium* plants in early stages. Then, we use the labeled points sampling method from [4], to obtain the corresponding point clouds.

The L-strings of the generated *Chenopodium Album* plants consist of 5 different modules: stem, cotyledon, petiole, leaf and branch. For each module, there is a different set of parameters that describe the organ represented by the module. The modules’ parameters are as follows:

- Stem: diameter, length, growing angle and phyllotaxis angle.
- Cotyledon: angle, length, nerve curvature factor.
- Petiole: starting diameter, ending diameter, angle, length, and elasticity factor.
- Leaf: nerve curvature factor, length and width.
- Branch: branching angle and elasticity factor.

The dataset contains plants of different shapes and structures, in a way that for each different structure there is a number of plants of different shapes. We ensure the balance between the different structures in the dataset by fixing the number of different plants for each structure, in order to avoid any bias towards certain structures. We generate plants of 33 different structures with 100 different plants for each structure, resulting in a dataset of 3300 pairs of L-Strings and point clouds. The dataset is split into training (80%), validation (10%) and test (10%) sets. Figure 5 shows examples of generated plants from the dataset.

We evaluate our method on a test set of point clouds of synthetic plants, that have structures seen in the training set. Additionally, we evaluate on the same test set with simulated Gaussian noise, and on monocular depth images of the set, to show our models robustness to acquisition noise and incomplete inputs.

Finally we make first tests of our method on 5 scans of real *Chenopodium Album* plants from [33], to test its ability to generalize to real data.



Figure 5: Examples of *Chenopodium Album* plants from our dataset.

## 6 Evaluation

This section presents the evaluation of our method with respect to three common phenotyping applications, namely 3D reconstruction, 3D skeleton extraction, and segmentation. For each application, we outline an evaluation protocol and compare to strong baselines.

### 6.1 Implementation Details

We implemented our method using Pytorch on Quadro RTX 5000 GPU. We learn a latent space  $\mathcal{S}$  of dimension  $dim_{\mathcal{S}} = 100$  with the recursive encoder-decoder pair architecture in Fig 2 of hidden layer size  $h_{recur} = 200$ , and the classifiers with a hidden layer  $h_{class} = 200$ . We optimize the weights of the network using Adam optimizer with a learning rate of 0.001, decaying by factor of 0.5 every 50 epochs. For the point cloud encoder we train a PointNet point regression network with Adam optimiser on a learning rate of 0.001. The weights of the layers of all the trained networks are initialized using Xavier uniform initialization.

Our method works on binary trees, while the L-String trees in our dataset mostly don’t have a bi-

Testset	Method	Accuracy	Completeness	Hausdorff	Silhouette	# Comp.
Synthetic	SIREN	<b>0.0035 <math>\pm</math> 0.024</b>	<b>0.001 <math>\pm</math> 0.0004</b>	<b>0.165 <math>\pm</math> 0.204</b>	0.0395 $\pm$ 0.01	34.1 $\pm$ 19.2
	Ours	0.0148 $\pm$ 0.019	0.0186 $\pm$ 0.021	0.595 $\pm$ 0.215	<b>0.0203 <math>\pm</math> 0.008</b>	<b>1</b>
Noise	SIREN	0.0156 $\pm$ 0.076	<b>0.0019 <math>\pm</math> 0.0006</b>	<b>0.324 <math>\pm</math> 0.327</b>	0.1425 $\pm$ 0.032	256.8 $\pm$ 69.4
	Ours	<b>0.014 <math>\pm</math> 0.017</b>	0.0182 $\pm$ 0.0186	0.598 $\pm$ 0.216	<b>0.0204 <math>\pm</math> 0.008</b>	<b>1</b>
Depth images	SIREN	<b>0.0098 <math>\pm</math> 0.123</b>	<b>0.0027 <math>\pm</math> 0.0029</b>	<b>0.428 <math>\pm</math> 0.437</b>	0.0485 $\pm$ 0.03	41.2 $\pm$ 20.5
	Ours	0.0165 $\pm$ 0.02	0.021 $\pm$ 0.035	0.615 $\pm$ 0.22	<b>0.0208 <math>\pm</math> 0.008</b>	<b>1</b>

Table 2: Comparison to SIREN [44] for the 3D reconstruction of plants from point clouds on our test sets of synthetic scans, noisy point clouds and depth images. We compare on geometric distance measures (accuracy, completeness and Hausdorff), and on perceptual and qualitative measures (silhouette error and the number of connected components, denoted # Comp.).

nary tree structure. We summarize the L-Strings into binary trees, by combining the modules that always occur together as individual nodes with concatenated parameter sets. In particular, we combine the two cotyledon modules into one Cotyledons node with 4 parameters. Stems are always followed by a petiole and a leaf, therefore we combine them in one node called Stem that has 12 parameters. In case of a branching, the branch module is combined with the stem, petiole and leaf modules to form a Branch node of 14 parameters. Finally, the first stem module of the tree forms a node on its own called Root of 3 parameters. Note that we do not duplicate the symmetric parameters in the cotyledons (first two), which explains the number of resulting parameters. As for the Root node, we do not include the angle parameter since it is fixed across all the plants.

For the segmentation experiment where we use the  $k$  nearest neighbors algorithm, we set  $k = 10$ . As for the reconstruction experiments, when using SIREN we need to input the point normals along with the point cloud, for this we use a normal estimation PCA-based method, which fits local planes to each point’s neighborhood.

## 6.2 3D Reconstruction

We quantitatively evaluate our method for 3D reconstruction of plants from input point clouds, on our test sets using five evaluation metrics. The first three are the commonly used metrics for 3D reconstruction methods, namely accuracy, completeness,

and Hausdorff distance. Accuracy and completeness are computed using the Chamfer distance between the ground truth point cloud and uniformly sampled points on the reconstructed surface. Accuracy measures how closely the reconstructed points lie to the ground truth, while completeness measures how well the reconstruction covers all parts of the ground truth’s geometry. Hausdorff distance measures the largest distances between the reconstructed and ground truth points, offering a worst-case assessment of the geometric alignment.

As these metrics are only based on 3D distances and do not account for the visual consistency of the reconstructions, we additionally consider the number of connected components that are reconstructed and silhouette error. The silhouette error is computed as the average pixel-wise absolute difference between the binary masks of the reconstructed and ground-truth meshes, rendered from multiple viewpoints. For each viewpoint, both meshes are rendered to produce binary images (silhouettes), where foreground pixels indicate visible parts of the shape. The error is then measured by taking the absolute value of the pixel-wise subtraction between the two silhouettes, averaged across all pixels and viewpoints (we use 400 viewpoints). This metric evaluates the visual similarity between the ground truth and the reconstructed mesh. Finally, the number of connected components measures global consistency and should be 1 for our dataset of isolated plants.

We compare our method to SIREN [44], an implicit neural representation method that uses sine activa-

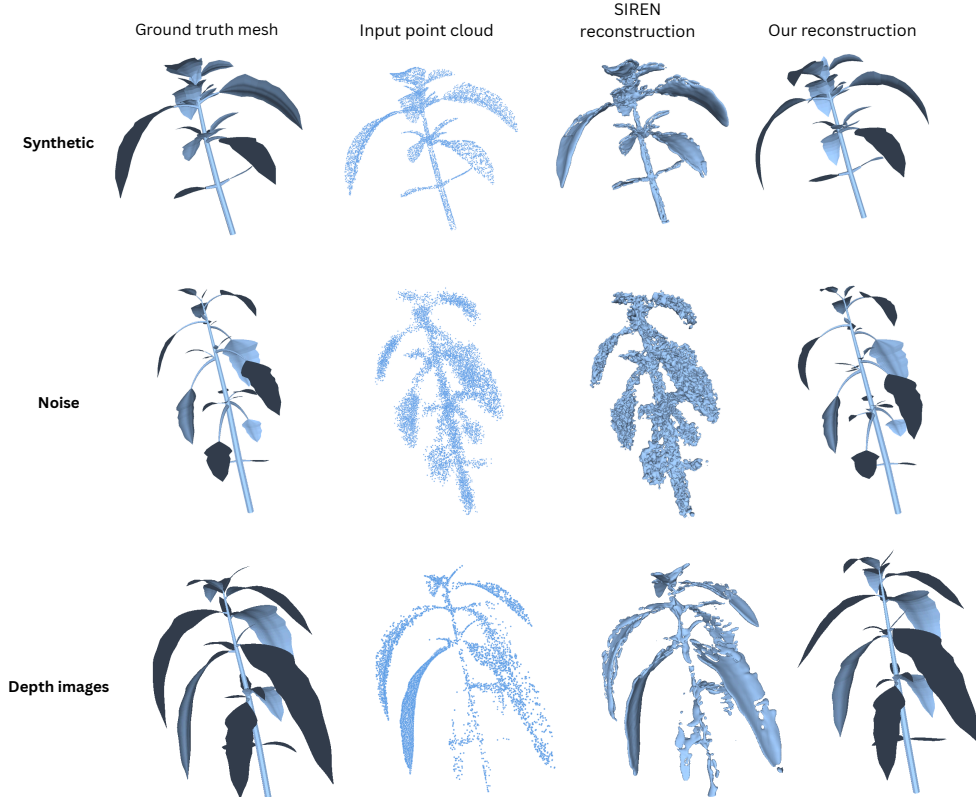


Figure 6: Qualitative results for 3D reconstruction by our method and SIREN [44], on synthetic clean, noisy and partial point clouds.

tion functions to model continuous signals, including signed distance functions (SDFs). For 3D reconstruction, the surface can be extracted as the zero level set of the SDF using Marching Cubes. SIREN was identified as the best-performing method for reconstructing plant geometry from point clouds by Prasad et al. [38], due to its ability to capture fine geometric details.

Our method produces a complete smooth mesh that captures the plant visual shape and is robust with respect to input noise and missing input. Table 2 shows the results, where one can note that SIREN performs well in terms of the 3D distance-based error measures accuracy, completeness and Hausdorff distance. SIREN’s performance degrades significantly for depth images, and even more for

noisy data. While our method has higher numerical error for these measurements than SIREN, it is much more robust to partial observations and noise. When considering silhouette loss, our method significantly outperforms SIREN as the visual similarity of the results is much higher for our method, (see Fig. 6). While the number of connected components of the reconstruction is always 1 for our method by construction, SIREN reconstructs highly fragmented shapes.

Fig. 6 shows examples of SIREN’s and our reconstructions for the three types of test examples. Note that while our reconstructions may have some misalignments, they are well structured and similar to the ground truth. In contrast, SIREN reconstructs fragmented shapes close to the input point clouds

that are globally dissimilar from the ground truth plants.

### 6.3 Skeletonization

	Synthetic	Noise	Depth images
[53]	$0.561 \pm 0.312$	$0.701 \pm 0.344$	$0.595 \pm 0.324$
[6]	$0.544 \pm 0.286$	$0.583 \pm 0.301$	$0.716 \pm 0.377$
[30]	$0.740 \pm 0.355$	$0.776 \pm 0.363$	-
Ours	<b><math>0.037 \pm 0.052</math></b>	<b><math>0.034 \pm 0.044</math></b>	<b><math>0.042 \pm 0.055</math></b>

Table 3: Comparison to Xu et al. [53], Chaudhury et al. [6], and Livny et al. [30] for 3D skeleton extraction in terms of Chamfer Distance. “-” means that the method crashed due to numerical problems.

We quantitatively evaluate our method for 3D skeleton extraction from input point cloud using the bidirectional Chamfer Distance. Chamfer Distance helps capturing the geometrical discrepancy between the ground truth skeleton and the predicted skeleton by measuring the sum of nearest neighbour distances in both directions.

We compare our method with two classical plant skeletonization baselines Livny et al. [30], Xu et al. [53] and a stochastic skeleton refinement method Chaudhury et al. [6] that takes a predicted skeleton as input and outputs a refined skeleton. In this comparison we apply the skeleton refinement on the output skeletons from applying Xu et al. [53] on the plant point clouds.

All these methods are designed to take scans of leafless plants as input. However, our dataset contains *Chenopodium Album* plants with leaves. Table 3 shows the results on the test sets of synthetic clean, noisy and partial point clouds. Our method shows consistent performance on the different test sets, suggesting robustness to noise and missing parts in the input point clouds for the skeletonization task. Since the baseline methods are not designed to take leaves as input, they tend to interpret leaf geometry as part of the skeleton, while the ground truth skeleton mainly describes the skeletal structure of the stem, branches and petioles. This explains the higher Chamfer distances, and the visual difference shown in Fig. 7.

### 6.4 Segmentation

We quantitatively evaluate our method’s performance on the semantic segmentation task applied to our test sets using standard classification metrics: precision, recall, F1 score, and Intersection over Union (IoU). For each class, precision is defined as the ratio of true positives to the sum of true positives and false positives, while recall is the ratio of true positives to the sum of true positives and false negatives. The F1 score is the harmonic mean of precision and recall. Finally, IoU is computed as the ratio of the intersection to the union of the predicted and ground truth point sets for a given class.

We compare our method to the two strong baselines PlantNet [26] and PSegNet [25]. Both PlantNet and PSegNet take a deep neural network approach with special sampling strategies, and are suitable for semantic and instance segmentation of plants.

Table 4 shows the results on the test sets of synthetic and noisy point clouds. We do not test segmentation methods on the depth image test set, as we do not have ground truth labels in this case. For synthetic scans, PSegNet outperforms all the methods except on Cotyledons segmentation, where our method shows a better performance. However, when noise is introduced, our method outperforms the other methods for most of the measures. Note that the petiole is the most difficult part to segment; this is because of its cylindrical shape, which is very close to the stem branches and makes it difficult to discriminate between these two classes. Overall, our method is robust to noise and performs on-par with the strong baselines.

Fig. 8 shows the semantic segmentation outputs of our method compared to the ground truth, where the semantics are properly captured even for noisy inputs. Furthermore, we show our method’s ability to perform instance segmentation in Fig. 9, where it successfully separates individual plant parts and remains robust to noise.

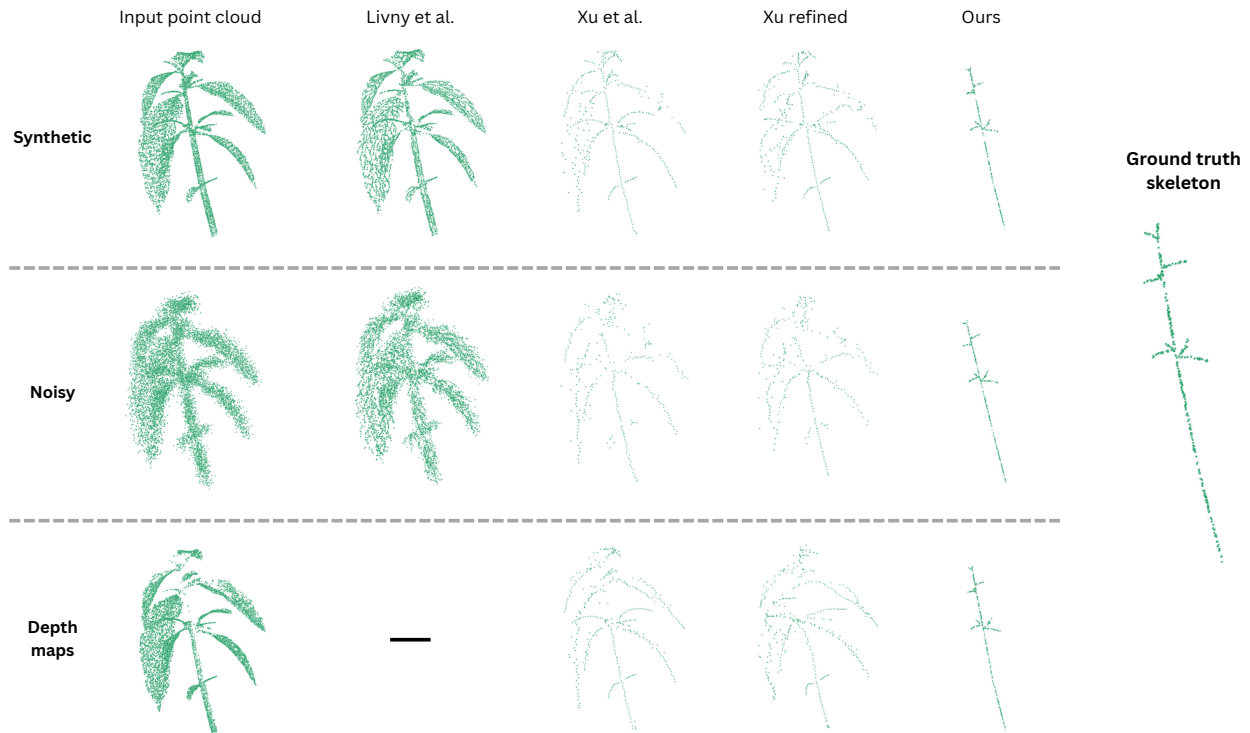


Figure 7: Qualitative results for skeletonization by our method, Livny et al. [30], Xu et al. [53], and Chaudhury et al. [6] refinement on Xu skeleton, from clean synthetic, noisy and partial point clouds taken from monocular depth maps. “-” means that the method crashed due to numerical problems.

## 7 Conclusion and Discussion

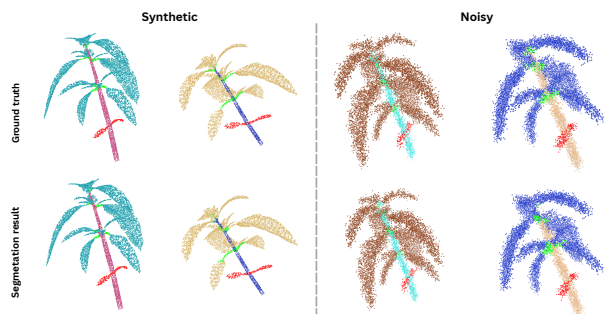


Figure 8: Examples of semantic segmentation results on synthetic clean and noisy point clouds.

In this paper we have presented a data-driven method to infer plants parametric representations i.e. L-Strings, from 3D unstructured point cloud input. We have shown that the L-String representation contains structural and geometric information that the input scans lack, and that such information allows for multiple tasks like 3D reconstruction, skeletonization and segmentation. Our results have shown that our method is on-par with the state-of-the-art for these tasks on synthetic data, and is robust to noisy and incomplete input. However, the performance of our method is limited to synthetic data, and first results from this first version of the method need to be qualitatively and quantitatively improved when applied to real scans.

	Stem				Leaf				Petiole				Cotyledons			
	Prec.	Rec.	F1	IoU	Prec.	Rec.	F1	IoU	Prec.	Rec.	F1	IoU	Prec.	Rec.	F1	IoU
<b>Synthetic</b>																
PlantNet	<b>91</b>	97	94	88	98	99	<b>99</b>	97	89	76	82	70	97	94	95	91
PSegNet	<b>91</b>	<b>99.5</b>	<b>95</b>	<b>90</b>	<b>99</b>	<b>99.6</b>	<b>99</b>	<b>98</b>	<b>95</b>	<b>88</b>	<b>92</b>	<b>85</b>	<b>99</b>	89	94	88
Ours	89	93	91	84	97	98	98	95	68	54	59	45	97	<b>98</b>	<b>97</b>	<b>94</b>
<b>Noise</b>																
PlantNet	88	81	84	73	93	99	96	91	75	32	45	29	74	<b>89</b>	80	68
PSegNet	<b>99</b>	75	85	74	90	<b>99.7</b>	95	90	<b>76</b>	21	33	20	<b>98</b>	80	88	79
Ours	85	<b>90</b>	<b>88</b>	<b>78</b>	<b>97</b>	97	<b>97</b>	<b>94</b>	60	<b>47</b>	<b>51</b>	<b>37</b>	93	<b>89</b>	<b>91</b>	<b>84</b>

Table 4: Comparison to PlantNet [26] and PSegNet [25] for semantic segmentation on synthetic and noisy points test sets using standard classification measures Precision, Recall, F1-Score and Intersection over Union (IoU). All values are percentages.

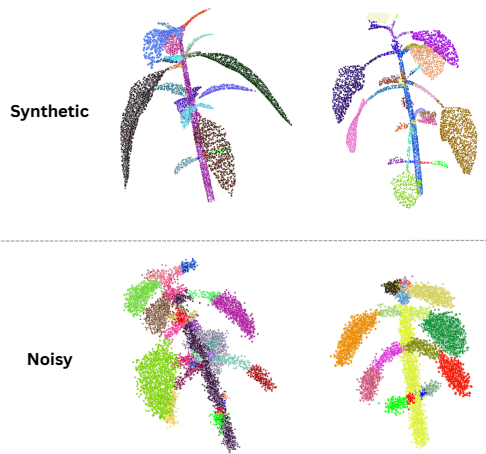


Figure 9: Examples of instance segmentation results on synthetic clean and noisy point clouds.

This work demonstrate the feasibility to learn latent space of 3D plant structures and reconstruct plant architecture parametric models from it. In the next step, our aim is to upscale our method to address fully real 3D plant point clouds. For this we need to investigate the level of accuracy required to simulated plants real plants so that the method can use simulated plants to learn real plant architectures. Fig 10 shows first tests of our 3D reconstructions from real scans. Although the reconstructions are not yet accurate on all levels, global information is learned by our model.

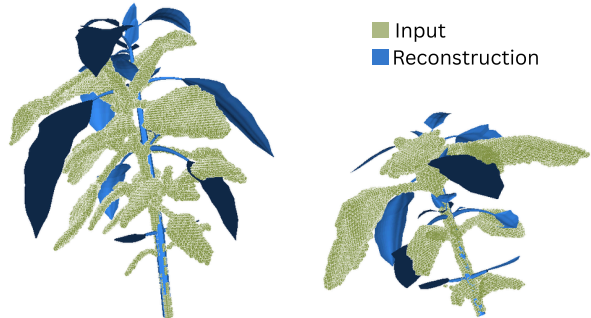


Figure 10: Our 3D reconstruction results on input scans of real *Chenopodium Album* plants.

## 8 Acknowledgements

We thank Franck Hétroy-Wheeler for helpful discussions, and Ayan Chaudhury, Frédéric Boudon, and Aymen Merrouche for providing support for their code. This work was partially supported by French government funding managed by the National Research Agency under grant ANR-24-CE23-1586 (4DPlants).

## References

- [1] H. Abelson and A. DiSessa. *Turtle geometry: The computer as a medium for exploring mathematics*. MIT press, 1986.

- [2] F. Boudon, C. Pradal, T. Cokelaer, P. Prusinkiewicz, and C. Godin. L-py: an l-system simulation framework for modeling plant architecture development based on a dynamic language. *Frontiers in plant science*, 3:76, 2012.
- [3] S. Chattopadhyay, S. A. Akbar, N. M. Elfiky, H. Medeiros, and A. Kak. Measuring and modeling apple trees using time-of-flight data for automation of dormant pruning applications. In *2016 IEEE Winter conference on applications of computer vision (WACV)*, pages 1–9. IEEE, 2016.
- [4] A. Chaudhury, F. Boudon, and C. Godin. 3d plant phenotyping: All you need is labelled point cloud data. In *European conference on computer vision*, pages 244–260. Springer, 2020.
- [5] A. Chaudhury and C. Godin. *Geometry Reconstruction of Plants*, pages 119–142. 09 2020.
- [6] A. Chaudhury and C. Godin. Skeletonization of plant point cloud data in stochastic optimization framework. *bioRxiv*, 2020.
- [7] A. Chaudhury, C. Ward, A. Talasaz, A. G. Ivanov, M. Brophy, B. Grodzinski, N. P. Hüner, R. V. Patel, and J. L. Barron. Machine vision system for 3d plant phenotyping. *IEEE/ACM transactions on computational biology and bioinformatics*, 16(6):2009–2022, 2018.
- [8] A. Chaudhury, C. Ward, A. Talasaz, A. G. Ivanov, N. P. Huner, B. Grodzinski, R. V. Patel, and J. L. Barron. Computer vision based autonomous robotic system for 3d plant growth measurement. In *2015 12th Conference on Computer and Robot Vision*, pages 290–296. IEEE, 2015.
- [9] L. Chuan-An, H.-H. Huang, Z.-Y. Chen, and H.-H. Chen. A unified RvNN framework for end-to-end Chinese discourse parsing. In D. Zhao, editor, *Proceedings of the 27th International Conference on Computational Linguistics: System Demonstrations*, pages 73–77, Santa Fe, New Mexico, Aug. 2018. Association for Computational Linguistics.
- [10] Y. Chéné, D. Rousseau, P. Lucidarme, J. Bertheloot, V. Caffier, P. Morel, Étienne Belin, and F. Chapeau-Blondeau. On the use of depth camera for 3d phenotyping of entire plants. *Computers and Electronics in Agriculture*, 82:122–127, 2012.
- [11] M. Cordier, P. Rasti, C. Torres, and D. Rousseau. Affordable phenotyping system for automatic detection of hypersensitive reactions. *Plant Phenomics*, 0(ja).
- [12] F. Costa, P. Frasconi, V. Lombardo, and G. Soda. Towards incremental parsing of natural language using recursive neural networks. *Applied Intelligence*, 19:9–25, 2003.
- [13] H. Dobbs, O. Batchelor, R. Green, and J. Atlas. Smart-tree: Neural medial axis approximation of point clouds for 3d tree skeletonization. In *Iberian Conference on Pattern Recognition and Image Analysis*, pages 351–362. Springer, 2023.
- [14] S. Du, R. Lindenbergh, H. Ledoux, J. Stoter, and L. Nan. Adtree: Accurate, detailed, and automatic modelling of laser-scanned trees. *Remote Sensing*, 11(18):2074, 2019.
- [15] H. Dutagaci, P. Rasti, G. Galopin, and D. Rousseau. Rose-x: an annotated data set for evaluation of 3d plant organ segmentation methods. *Plant Methods*, 16, 2020.
- [16] P. Feldman, M. Fainstein, V. Siless, C. Delrieux, and E. Iarussi. Vesselvae: Recursive variational autoencoders for 3d blood vessel synthesis. In H. Greenspan, A. Madabhushi, P. Mousavi, S. Salcudean, J. Duncan, T. Syeda-Mahmood, and R. Taylor, editors, *Medical Image Computing and Computer Assisted Intervention – MICCAI 2023*, pages 67–76, Cham, 2023. Springer Nature Switzerland.
- [17] L. Gao, J.-M. Sun, K. Mo, Y.-K. Lai, L. J. Guibas, and J. Yang. Scenehgn: Hierarchical graph networks for 3d indoor scene generation with fine-grained geometry. *IEEE Transactions on Pattern Analysis and Machine Intelligence*, 45(7):8902–8919, 2023.
- [18] M. Ghahremani, K. Williams, F. Corke, B. Tideman, Y. Liu, X. Wang, and J. H. Doonan. Direct and accurate feature extraction from 3d point clouds of plants using ransac. *Computers and Electronics in Agriculture*, 187:106240, 2021.
- [19] C. Godin. Representing and encoding plant architecture: a review. *Annals of forest science*, 57(5):413–438, 2000.
- [20] C. Godin and P. Ferraro. Quantifying the degree of self-nestedness of trees: application to the structural analysis of plants. *IEEE/ACM transactions on computational biology and bioinformatics / IEEE, ACM*, 7(4):688 – 703, 10 2010.



- [21] C. Godin and H. Sinoquet. Functional-structural plant modelling. 2005.
- [22] S. González-Domínguez, J. Balado, A. Novo, and P. Arias. Tree digitisation from point clouds with unreal engine. *ISPRS Annals of the Photogrammetry, Remote Sensing and Spatial Information Sciences*, 10:555–560, 2023.
- [23] J. Guo, H. Jiang, B. Benes, O. Deussen, X. Zhang, D. Lischinski, and H. Huang. Inverse procedural modeling of branching structures by inferring l-systems. *ACM Transactions on Graphics (TOG)*, 39(5):1–13, 2020.
- [24] J. J. Lee, B. Li, and B. Benes. Latent l-systems: Transformer-based tree generator. *ACM Trans. Graph.*, 43(1), nov 2023.
- [25] D. Li, J. Li, S. Xiang, and A. Pan. Psegnet: Simultaneous semantic and instance segmentation for point clouds of plants. *Plant Phenomics*, 2022, 2022.
- [26] D. Li, G. Shi, J. Li, Y. Chen, S. Zhang, S. Xiang, and S. Jin. Plantnet: A dual-function point cloud segmentation network for multiple plant species. *ISPRS Journal of Photogrammetry and Remote Sensing*, 184:243–263, 2022.
- [27] J. Li, K. Xu, S. Chaudhuri, E. Yumer, H. Zhang, and L. Guibas. Grass: generative recursive autoencoders for shape structures. *ACM Trans. Graph.*, 36(4), July 2017.
- [28] M. Li, A. G. Patil, K. Xu, S. Chaudhuri, O. Khan, A. Shamir, C. Tu, B. Chen, D. Cohen-Or, and H. Zhang. Grains: Generative recursive autoencoders for indoor scenes, 2019.
- [29] Y. Liu, J. Guo, B. Benes, O. Deussen, X. Zhang, and H. Huang. Treepartnet: Neural decomposition of point clouds for 3d tree reconstruction. *ACM Transactions on Graphics (Proceedings of SIGGRAPH Asia)*, 40(6):232:1–232:16, 2021.
- [30] Y. Livny, F. Yan, M. Olson, B. Chen, H. Zhang, and J. El-Sana. Automatic reconstruction of tree skeletal structures from point clouds. In *ACM SIGGRAPH Asia 2010 papers*, pages 1–8. 2010.
- [31] K. Mertoğlu, Y. Şalk, S. K. Sarıkaya, K. Turgut, Y. Evrenesoğlu, H. Çevikalp, Ömer Neziğ Gerek, H. Dutağacı, and D. Rousseau. Planest-3d: A new annotated dataset for segmentation of 3d plant point clouds, 2024.
- [32] L. Meyer, A. Gilson, O. Scholz, and M. Stamminger. Cherrypicker: Semantic skeletonization and topological reconstruction of cherry trees. In *2023 IEEE/CVF Conference on Computer Vision and Pattern Recognition Workshops (CVPRW)*. IEEE, June 2023.
- [33] K. Mirande, C. Godin, M. Tisserand, J. Charlaix, F. Besnard, and F. Héty-Wheeler. A graph-based approach for simultaneous semantic and instance segmentation of plant 3d point clouds. *Frontiers in Plant Science*, 13:1012669, 2022.
- [34] K. Mirande, C. Godin, M. Tisserand, J. Charlaix, F. Besnard, and F. Héty-Wheeler. Point cloud data sets of real and virtual chenopodium alba, Aug. 2022.
- [35] C. Niu, J. Li, and K. Xu. Im2struct: Recovering 3d shape structure from a single rgb image. In *Proceedings of the IEEE Conference on Computer Vision and Pattern Recognition (CVPR)*, June 2018.
- [36] A. Paproki, X. Sirault, S. Berry, R. Furbank, and J. Fripp. A novel mesh processing based technique for 3d plant analysis. *BMC plant biology*, 12:1–13, 2012.
- [37] S. Paulus. Measuring crops in 3d: using geometry for plant phenotyping. *Plant Methods*, 15, 09 2019.
- [38] A. D. Prasad, A. Jignasu, Z. Jubery, S. Sarkar, B. Ganapathysubramanian, A. Balu, and A. Krishnamurthy. Deep implicit surface reconstruction of 3d plant geometry from point cloud. In *AI for Agriculture and Food Systems*.
- [39] C. Preuksakarn, F. Boudon, P. Ferraro, J.-B. Durand, E. Nikinmaa, and C. Godin. Reconstructing plant architecture from 3d laser scanner data. *Proceedings of the 6th International Workshop on Functional-Structural Plant Models*, 09 2010.
- [40] P. Prusinkiewicz and A. Lindenmayer. The algorithmic beauty of plants. In *The Virtual Laboratory*, 1990.
- [41] S. Pv. *Introduction to Unreal Engine 4*, pages 1–20. 01 2021.
- [42] C. R. Qi, H. Su, K. Mo, and L. J. Guibas. Pointnet: Deep learning on point sets for 3d classification and segmentation. *CoRR*, abs/1612.00593, 2016.
- [43] A. Runions, B. Lane, and P. Prusinkiewicz. Modeling trees with a space colonization algorithm. pages 63–70, 01 2007.

- [44] V. Sitzmann, J. N. P. Martel, A. W. Bergman, D. B. Lindell, and G. Wetzstein. Implicit neural representations with periodic activation functions, 2020.
- [45] R. Socher, C. C. Lin, C. Manning, and A. Y. Ng. Parsing natural scenes and natural language with recursive neural networks. In Proceedings of the 28th international conference on machine learning (ICML-11), pages 129–136, 2011.
- [46] R. Socher, C. D. Manning, and A. Y. Ng. Learning continuous phrase representations and syntactic parsing with recursive neural networks. In Proceedings of the NIPS-2010 deep learning and unsupervised feature learning workshop, volume 2010, pages 1–9. Vancouver, 2010.
- [47] O. Štáva, B. Beneš, R. Měch, D. G. Aliaga, and P. Křištof. Inverse procedural modeling by automatic generation of l-systems. In Computer graphics forum, volume 29, pages 665–674. Wiley Online Library, 2010.
- [48] O. Stava, S. Pirk, J. Kratt, B. Chen, R. Měch, O. Deussen, and B. Benes. Inverse procedural modelling of trees. In Computer Graphics Forum, volume 33, pages 118–131. Wiley Online Library, 2014.
- [49] K. Turgut, H. Dutagaci, G. Galopin, and D. Rousseau. Segmentation of structural parts of rosebush plants with 3d point-based deep learning methods. Plant Methods, 18(1):20, 2022.
- [50] K. Turgut, H. Dutagaci, and D. Rousseau. Rosegnet: An attention-based deep learning architecture for organ segmentation of plants. Biosystems Engineering, 221:138–153, 2022.
- [51] M. Wahabzada, S. Paulus, K. Kersting, and A.-K. Mahlein. Automated interpretation of 3d laser-scanned point clouds for plant organ segmentation. BMC Bioinformatics, 16:248, 08 2015.
- [52] A. Walter, F. Liebisch, and A. Hund. Plant phenotyping: From bean weighing to image analysis. Plant Methods, 11:14, 03 2015.
- [53] H. Xu, N. Gossett, and B. Chen. Knowledge and heuristic-based modeling of laser-scanned trees. ACM Trans. Graph., 26(4):19–es, Oct. 2007.
- [54] D.-M. Yan, J. Wintz, B. Mourrain, W. Wang, F. Boudon, and C. Godin. Efficient and robust reconstruction of botanical branching structure from laser scanned points. In 2009 11th IEEE International Conference on Computer-Aided Design and Computer Graphics, pages 572–575, 2009.
- [55] F. Yu, K. Liu, Y. Zhang, C. Zhu, and K. Xu. Partnet: A recursive part decomposition network for fine-grained and hierarchical shape segmentation. In Proceedings of the IEEE/CVF Conference on Computer Vision and Pattern Recognition (CVPR), June 2019.